Ion track formation and porosity in InSb induced by swift heavy ion irradiation ⓔⓟ

Taleb Alwadi ✉ ⓘ ; Christian Notthoff ⓘ ; Shankar Dutt ⓘ ; Jessica Wierbik ⓘ ; Nahid Afrin ⓘ ;
Alexander Kiy ⓘ ; Patrick Kluth ⓘ

Check for updates

View Online   Export Citation   CrossMark

Articles You May Be Interested In

Wavelet transform in stock prices forecasting and related financial data

AIP Conference Proceedings (March 2023)

Formation of TiO_2 nanorods by ion irradiation

J. Appl. Phys. (May 2014)

Field analysis of revealing the performance of vehicle trips at short and long-term traffic system

AIP Conference Proceedings (July 2023)

Ion track formation and porosity in InSb induced by swift heavy ion irradiation EP

Taleb Alwadi,[1,a] Christian Notthoff,[1,2] Shankar Dutt,[1] Jessica Wierbik,[1] Nahid Afrin,[1]
Alexander Kiy,[1] and Patrick Kluth[1]

AFFILIATIONS

[1]Department of Materials Physics, Research School of Physics, The Australian National University, Canberra, ACT 2601, Australia
[2]Department of Nuclear Physics and Accelerator Applications, Research School of Physics, The Australian National University, Canberra, ACT 2601, Australia

[a]Author to whom correspondence should be addressed: Taleb.Alwadi@anu.edu.au

ABSTRACT

Ion track formation, irradiation-induced damage (amorphization), and the formation of porosity in InSb after 185 MeV ^{197}Au swift heavy ion irradiation are studied as a function of ion fluence and irradiation angle. Rutherford backscattering spectrometry in channeling geometry reveals an ion track radius of about 16 nm for irradiation normal to the surface and 21 nm for off-normal irradiation at 30° and 60°. Cross-sectional scanning electron microscopy shows significant porosity that increases when irradiation was performed off-normal to the surface. Off-normal irradiation shows a preferential orientation of the pores at about 45° relative to the surface normal. Moreover, when subjected to identical conditions, InSb samples demonstrate notably higher swelling compared to GaSb bulk samples.

I. INTRODUCTION

The interaction of ions with matter is an energy-dependent process. In the low-energy regime, from keV to low-MeV energies, the ions deposit energy mainly via inelastic collisions with the target nuclei, a process known as nuclear stopping. In contrast, ions with higher energies in the order of tens to hundreds of MeV interact predominantly with the target electrons, a process known as electronic stopping;[1] any energies in between those two regimes are considered medium energy. The fabrication of porous semiconductors using heavy ion irradiation in both energy regimes has many interesting contemporary applications, including bioelectronic devices, nanophotonics, nanoelectronics, and thermoelectric devices.[2,3] Indium Antimonide (InSb) and Gallium Antimonide (GaSb) are III–V semiconductors with a narrow bandgap and high mobility.[4] One of the features of InSb is that it can be rendered porous upon heavy ion irradiation in the low-energy regime[5–7] and the medium energy regime[2] similar to GaSb[7] and Ge.[10] The induced porosity in the target material depends on the ion species and energy and is generally accompanied by amorphization of the material.[2,9] In the low-energy regime, where nuclear stopping is the predominant process, the formation of the pores occurs as a result

of vacancy clustering from the irradiation-induced production of point defects. The vacancy clustering is attributed to inefficient Frenkel pair recombination.[5,8] The transformation to the porous microstructure in InSb and GaSb occurs simultaneously with the crystalline to amorphous transformation. Kluth *et al.* show that InSb single crystalline wafers exhibit porosity after implantation with 1 MeV ^{69}Ga$^+$ ions with fluences up to 1×10^{15} ions/cm^2. The porosity started with the spherical void formation at lower fluence (1×10^{14} ions/cm^2), which increased in size with increasing irradiation fluence and led to the development of a spongelike structure at 2.5×10^{14} ions/cm^2. At 1×10^{15} ions/cm^2, the material's microstructure resembled a network of straight rods approximately 20 nm in diameter.[11] Datta *et al.* found that InSb wafers irradiated with 60 keV Ar$^+$ ions at a high fluence range of 1×10^{17} to 3×10^{18} ions/cm^2 showed the formation of nanoporous structures in the form of interconnected nanofibrous networks for irradiation normal to the surface and platelike structures for irradiation off-normal to the surface.[5]

In the middle energy regime, Giulian *et al.* studied InSb films grown by magnetron sputtering on SiO$_2$/Si substrates with various thicknesses from 20 to 300 nm. Results show that InSb with film

thickness up to 75 nm is amorphous, and above this thickness, the InSb films are polycrystalline with a zinc-blende structure. The samples were irradiated with 17 MeV Au ions, where the electronic energy loss is about 2.9 keV/nm, and the nuclear energy loss is about 1.4 keV/nm. Upon irradiation with fluences exceeding 1×10^{14} ions/cm^2, the structure of the thin films changes from amorphous into a polycrystalline foam. The porosity induced in InSb begins as small spherical voids with a diameter of approximately 2–3 nm, exhibiting highly damaged crystalline structures. As the irradiation fluence increases, small voids merge, forming a polycrystalline solid foam with open cells.[2]

In the high-energy regime, the predominant energy loss process is the inelastic interaction of the projectile ions with the target electrons, which induces a high density of electronic excitations and ionizations along the ion path.[12] Previous reports show the formation of porous structures using high-energy irradiation in amorphous Ge[12] and GaSb.[17,19] However, no previous work was found in the literature for swift heavy ion-induced porosification of InSb, and only two reports mention ion tracks in InSb, one by Szenes et al.[13] and another reported by Kamarou et al.[14]

This study investigates ion track formation and porosification in InSb after irradiation with 185 MeV ^{197}Au ions at various fluences. In addition, a comparison between the processes in InSb and GaSb will be discussed. Rutherford backscattering spectrometry in channeling geometry (RBS/C) was used to study track formation and material damage/amorphization. Furthermore, the effects of ion irradiation on the microstructure of the samples at high fluences were studied using scanning electron microscopy (SEM).

II. EXPERIMENTAL METHODS

Bulk InSb samples were used for this study for the damage track formation investigations using RBS/C and 2.2 μm thick InSb layers grown by metal-organic chemical vapor deposition (MOCVD) onto (001) GaAs substrates for porosity and swelling measurements. The InSb samples were irradiated at the Australian National University Heavy Ion Accelerator Facility at room temperature with 185 MeV ^{197}Au ions. The electronic energy loss for ^{197}Au ions in InSb was estimated using SRIM-2013 (Ref. 16) to 21 keV/nm with a mean ion range of 17 μm. The irradiation process was performed with the irradiation normal to the surface (0° irradiation angle), 30° and 60° relative to the surface normal. Irradiation fluences ranged from 8.8×10^{10} to 5.6×10^{13} ions/cm^2. The 2.2 μm thick InSb layers ensure that the electronic stopping is approximately constant over the full depth of the layer with negligible nuclear stopping for both normal and off-normal to the surface irradiations. The irradiated bulk samples were studied using Rutherford backscattering spectrometry in channeling configuration (RBS/C) using 2 MeV He^2 ions, and a surface barrier detector positioned at a scattering angle of 168°. To investigate swelling and microstructural changes in the samples after heavy ion irradiation scanning electron microscopy [FEI Verios 460 (SEM) with Gatan MonoCL 4 and Oxford EDS] was used. The samples were cleaved and imaged in cross-sectional geometry. Optical profilometry (Wyko NT9100 Surface Profiler) was used to measure the swelling of the irradiated samples.

III. RESULTS AND DISCUSSION

A. Damage cross section and track radius

In this section, we present results on the damage buildup in InSb as a function of irradiation fluence, which leads to the transition from crystalline to amorphous/porous material. Bulk InSb samples irradiated with 185 MeV ^{197}Au ions at fluences ranging from 8.8×10^{10} to 1.2×10^{12} ions/cm^2 were examined by RBS/C using 2 MeV He^2, which allows approximately 2 μm analysis depth. This is much smaller than the ion range of about 17 μm in InSb, and the energy loss is considered constant over that depth.

Figure 1 shows RBS/C spectra for samples irradiated at three different irradiation angles: (a) normal to the surface, (b) 30°, and (c) 60° with respect to the surface normal. An unirradiated InSb
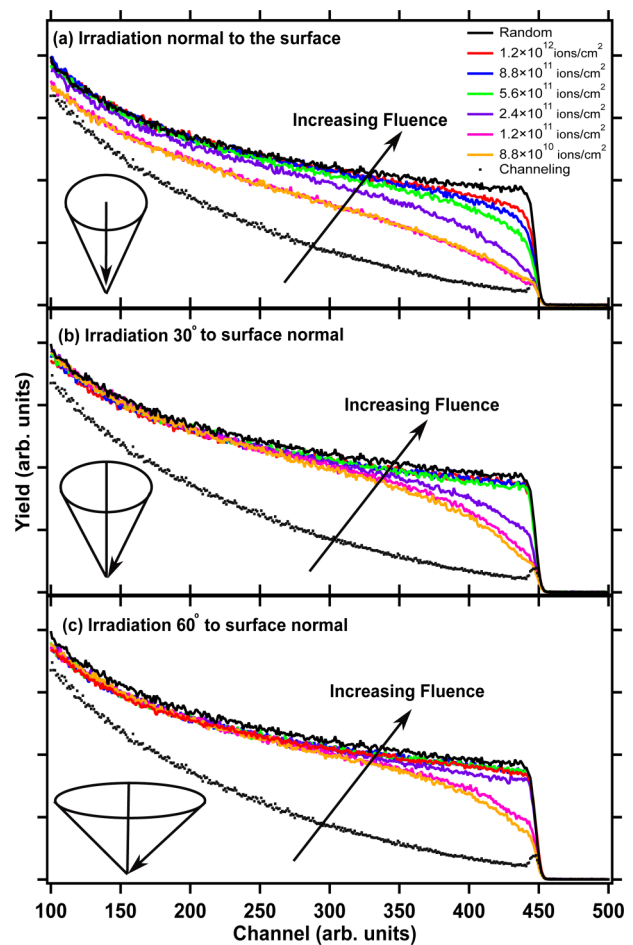
FIG. 1. RBS/C backscattering yield for InSb samples irradiated with 185 MeV ^{197}Au ions at varying ion fluences (8.8×10^{10}, 1.2×10^{11}, 2.4×10^{11}, 5.6×10^{11}, 8.8×10^{11}, and 1.2×10^{12} ions/cm^2), irradiated (a) normal to the surface and (b) 30° and (c) 60° tilted with respect to the surface normal. The black and dotted black lines correspond to the random and channeled orientation, respectively, for an unirradiated InSb sample.

23 October 2023 20:14:17

sample has been used as a reference sample for channeling and random configurations shown in Fig. 1 as a dotted-black line and a solid black line, respectively. It is apparent that the backscattering yield increases continually with increasing irradiation fluence, which is related to damage buildup in the material. The RBS spectra suggest that the material is amorphized at high fluences for samples irradiated off-normal to the surface as the channeling spectra almost resemble those in random configuration.

Quantitatively, the damage fraction of the damaged material as a function of fluence can be calculated as[16]

$$f_d(\varphi) = \frac{Y(\varphi) - Y_c}{Y_r - Y_c}, \qquad (1)$$

where $Y(\varphi)$ is the integrated backscattering yield between channels 100 and 500 for the different irradiated samples, Y_c is the integrated backscattering yield for the reference sample in channeling configuration, and Y_r is the integrated backscattering yield for the reference sample in a random configuration.

Figure 2(a) shows the damage fraction f_d of damaged InSb as a function of fluence φ extracted from the RBS/C spectra together with a fit to the Poisson law,

$$f_d(\varphi) = 1 - e^{-\sigma\left(\frac{\varphi}{\cos(\theta)}\right)}, \qquad (2)$$

where σ is the damage cross section and θ is the incident ion angle relative to the surface normal.[16,17]

The damage buildup as a function of irradiation fluence can be fitted well for irradiation normal to the surface with a damage cross section of $(8.7 \pm 0.6) \times 10^{-12}$ cm^2 and for an off-normal irradiation of $(1.4 \pm 0.1) \times 10^{-11}$ cm^2. Assuming that the ion tracks have a cylindrical shape with a homogeneous cross section,[14,17] the ion track radius r can be obtained from the damage cross section σ and amounts to (16 ± 4) nm for irradiation normal to the surface and (21 ± 6) nm for irradiation at 30° and 60° with respect to the surface normal.

Figure 2(b) shows the comparison of the damage buildup as a function of fluence for InSb and GaSb after irradiation with 185 MeV ^{197}Au ions normal to the surface. The RBS/C data for GaSb were obtained from our previous work.[16] It is apparent that the damage rate for InSb under identical irradiation conditions is significantly higher than for GaSb. For GaSb, the ion track radius was found to be (3 ± 0.8) nm for normal incidence and (5 ± 1) nm for off-normal incidence. This is a factor of four to five times smaller than for InSb. The smaller radius for the case of irradiation normal to the surface compared to tilted irradiation is likely related to channeling similar to the case of GaSb.[16] Previously, a track radius of 13 nm for InSb irradiated with Pb ions at 1.85 MeV/nucleon, corresponding to an energy loss of 28 keV/nm, was reported by Szenes *et al.* based on RBS/C investigations in channeling geometry, however, without showing any experimental details.[13] Nevertheless, the reported track radius by Szenes *et al.*[13] for InSb is in good agreement with our finding of a track radius of (16 ± 4) nm, which corresponds to an energy loss of 21 keV/nm for 0.94 MeV/nucleon Au ions used here. Another track radius of about 4.5 nm to about 9 nm has been reported by Kamarou *et al.*
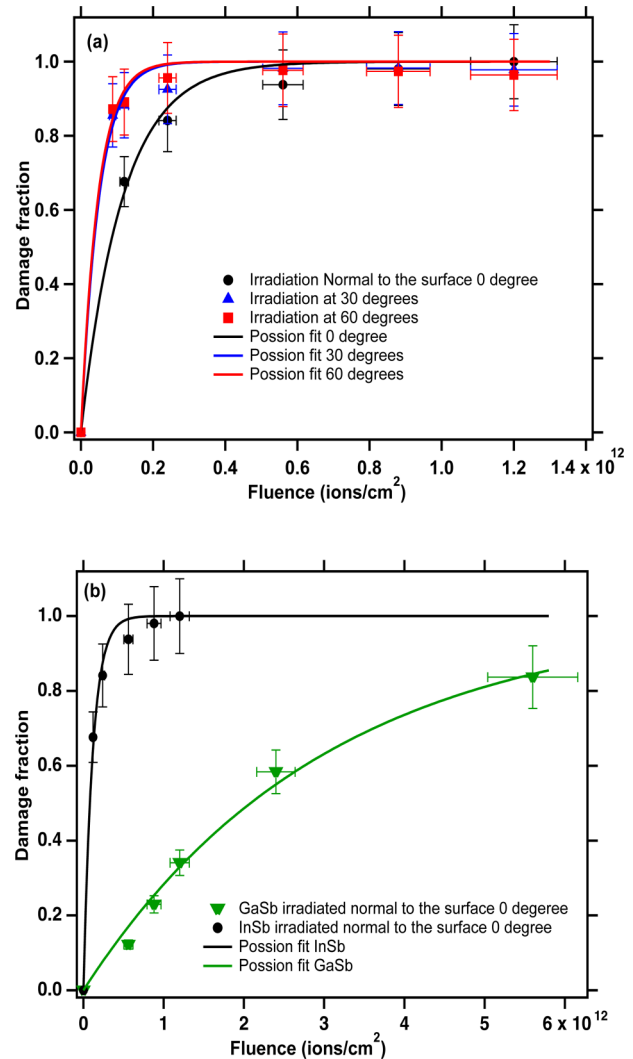
FIG. 2. (a) Damage fraction as a function of fluence for InSb samples irradiated normal to the surface, 30°, and 60° relative to the surface normal. (b) Damage buildup as a function of fluence for InSb and GaSb samples irradiated normal to the surface with 185 MeV ^{197}Au ions (Ref. 17). The solid lines fit the Poisson model equation (2).

for InSb irradiated with 2.9 MeV/nucleon Au ions, corresponding to an energy loss of 30 keV/nm, using transmission electron microscopy (TEM).[14]

B. Porous microstructure and swelling

In this section, we present the effects of ion irradiation on the microstructural changes of InSb films and point out the differences and similarities between InSb and GaSb irradiated under the same conditions. The GaSb results are part of our previous work.[16]

Figure 3(a) shows cross-sectional SEM images of InSb irradiated normal to the surface with fluences ranging from 5.6×10^{12} to

23 October 2023 20:14:17

5.6×10^{13} ions/cm^2. At a fluence of 5.6×10^{12} ions/cm^2, the emergence of irregularly shaped, separated voids with no preferential orientation can be observed. At a fluence of 8.8×10^{12} ions/cm^2, the pore size has increased in random directions. At higher fluences, the pores show an increasingly irregular pattern and start to join and form an irregular foamlike structure. At the highest fluence (5.6×10^{13} ions/cm^2), the material is characterized by nanosized sheets connected by fiberlike structures. The measured sheet thickness is approximately (58 ± 9) nm.

Figure 3(b) shows cross-sectional SEM images of InSb irradiated under an angle of 30° relative to the surface normal for the same irradiation fluences. Compared to the irradiation at normal incidence, the porosity proceeds with larger uniaxial swelling, and the pores show preferential orientation. It is worth noting that the pores are not aligned along the ion beam direction, but rather they are oriented at approximately 45° relative to the surface normal, in

the opposite direction to the incoming ion beam. Furthermore, at high irradiation fluence, the pore morphology for the samples irradiated at 30° is considerably different with a more fiberlike irregular microstructure.

Figures 4(a) and 4(b) show a comparison of the microstructural changes of InSb and GaSb, respectively, after swift heavy ion irradiation with ^{197}Au ions at 185 MeV. In InSb, the changes in the microstructure occur at a higher rate than GaSb. The pore size in InSb is larger than in GaSb at comparable fluences with more irregular shapes and random orientation. We attribute this result to the damage track formed in InSb being almost four to five times larger than the ion track in GaSb.

Figure 4(c) shows a cross-sectional SEM image of InSb irradiated at a 30° irradiation angle relative to the surface normal at a fluence of 1.2×10^{13}. Figure 4(d) shows a cross-sectional SEM image of GaSb irradiated at a 30-degree irradiation angle relative to the surface normal at a fluence of 8.8×10^{13} ions/cm^2. The main difference between the normal incidence irradiation and irradiation at an angle is the preferential orientation of the elongated pores as
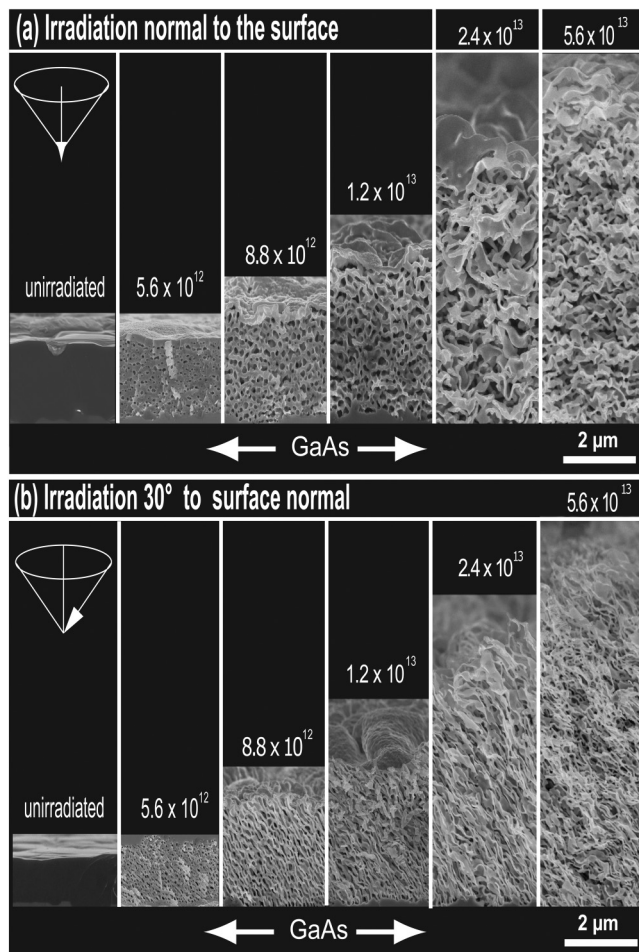
FIG. 3. Cross-sectional SEM images of InSb on GaAs substrates irradiated (a) normal to the surface (0°) and (b) at 30° relative to the surface normal as a function of irradiation fluence.

FIG. 4. Cross-sectional SEM images of (a) InSb irradiated normal to the surface at various fluences, (b) GaSb irradiated normal to the surface at various fluences, (c) InSb irradiated off-normal to the surface with an irradiation angle (30°) at an irradiation fluence of 1.2×10^{13} ions/cm^2, and (d) GaSb irradiated with 8.8×10^{13} ions/cm^2 at an irradiation angle of 30° with respect to the surface normal.

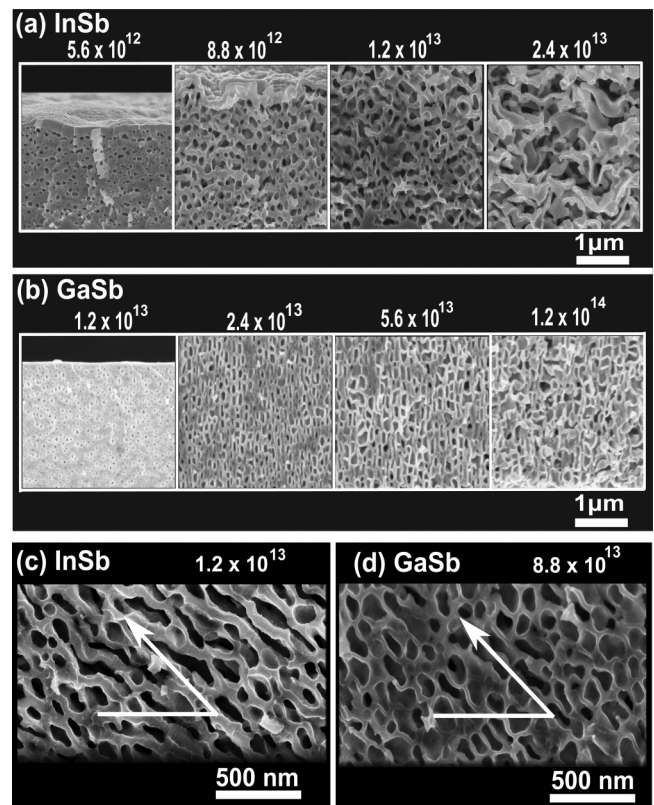described previously by Notthoff *et al.* for GaSb.[16] Interestingly, the pores are oriented at about 45° relative to the surface normal. InSb has the same preferential orientation as GaSb except that the elongated pores have sizes similar to GaSb at a lower ion fluence. The preferential orientation of the pores after ion irradiation in the InSb samples is independent of the irradiation angle, and it is due to the ion hammering effect and related to the strain and stress induced by the ion beam, as previously seen in GaSb.[16]

Previously, Kluth *et al.* demonstrated that a single ion impact into crystalline GaSb creates vacancy clusters, which then aggregate/grow into bigger voids via diffusion. However, macroscopic voids and noticeable swelling were only observable above a threshold fluence, which roughly corresponds to a complete coverage of the sample with ion tracks and an almost entirely amorphized sample.[18] We observe a similar process in InSb, which also shows a threshold fluence for observable swelling, corresponding to almost complete coverage of the sample with ion tracks.

Strong porosification is only observed for irradiation beyond the threshold fluence where the InSb and GaSb samples are rendered amorphous. The vacancy clusters at the beginning of irradiation serve as precursors of free volume in the amorphous phase, which then coalesces to create larger voids. For further information about the free volume model of the amorphous phase, see Refs. 20–22.

The volume fraction of voids (porosity) as a function of irradiation fluence $f_v(\varphi)$ can be described using[16]

$$f_v(\varphi) = f_o \left[1 - e^{-\frac{k}{\cos(\theta)}(\varphi - \varphi_o \cos(\theta))} \right], \quad (3)$$

where f_o is the maximum porosity, k is an effective ion cross section, φ_o is the threshold fluence above which the measurable swelling can be observed, and $\cos(\theta)$ is a correction for the ion path length due to the incident angle of ions. Assuming uniaxial expansion, the porosity $f_v(\varphi)$ can be converted into the swelling $\Delta h(\varphi)$ by

$$\Delta h(\varphi) = h(\varphi) - h_\circ = h_\circ \left(\frac{f_v(\varphi)}{1 - f_v(\varphi)} \right), \quad (4)$$

where $h_\circ$ is the initial sample thickness and $f_v(\varphi)$ can be determined using Eq. (3). Equation (4) was used to fit the data in Fig. 5(a), where the GaSb swelling data were obtained from Notthoff *et al.*[16]

Figure 5(a) shows the swelling, normalized to the initial film thickness, for InSb and GaSb thin films, to be able to compare the measurements for different film thicknesses. InSb and GaSb thin films were irradiated with [197]Au ions at 185 MeV normal to the surface. The solid lines in Fig. 5(a) represent the best fit of Eq. (4) to the data. The threshold fluence for InSb was determined from the fit to be about $(1.0 \pm 0.4) \times 10^{12}$ ions/cm^2, maximum porosity $f_o \approx 0.810 \pm 0.003$, and effective ion cross section $k \approx (9.95 \pm 0.37)$ nm^2, which is much smaller than the damage cross section ($\sigma = 866.5$ nm^2) and almost three times larger than in GaSb. In contrast, GaSb swelling data reproduced from Notthoff *et al.*[16] show a threshold fluence of about 5×10^{12} ions/cm^2 above which swelling can be observed, maximum porosity $f_o \approx 0.55 \pm 0.01$, and an effective ion cross section $k \approx (3.4 \pm 0.4)$ nm^2. The reported damage cross section in GaSb was 33 nm^2.
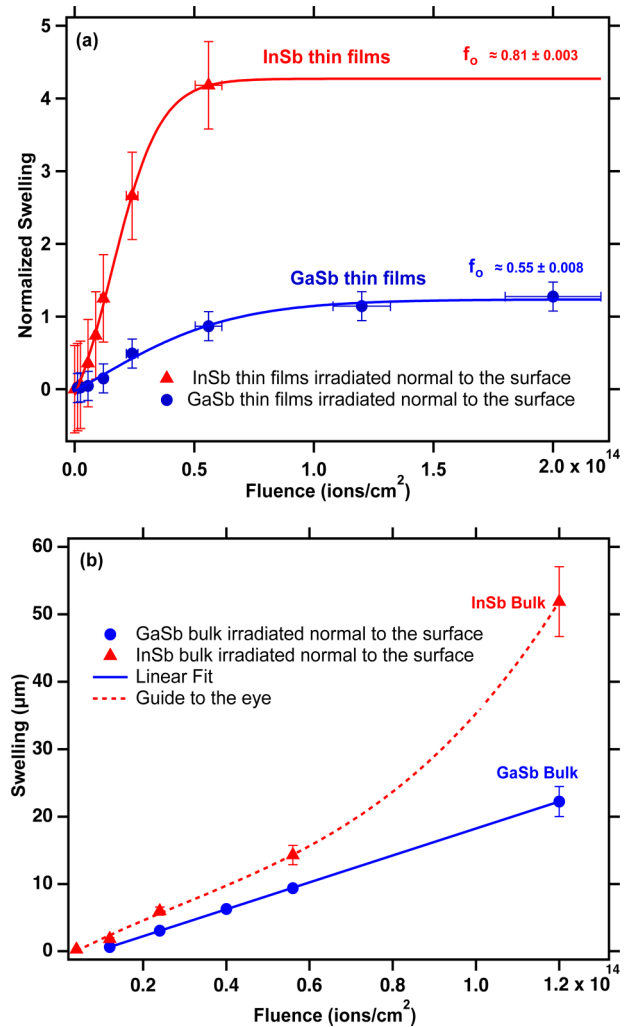

FIG. 5. (a) Normalized swelling of porous InSb and GaSb thin films irradiated normal to the surface with 185 MeV [197]Au ions as a function of fluence and the best fits to Eq. (4) (solid lines). (b) Swelling of bulk InSb (triangles) and bulk GaSb (circles) as a function of irradiation fluence. The solid line is the linear fit for GaSb, and the dashed line is a guide to the eye for InSb.

Based on RBS/C measurements in Sec. III A, we observed approximately 97% amorphization of InSb samples at a fluence of about 5.0×10^{11} ions/cm^2, which corresponds almost to complete coverage of the sample with ion tracks, which is somewhat below our observed threshold fluence for the formation of porosity φ_o that was determined from the fit in Fig. 5(a). The coverage of ion tracks of the irradiated area was determined using the overlap model,[22]

$$A = 1 - e^{(-\varphi_o \pi r^2)}, \quad (5)$$

where φ_o is the threshold fluence and r is the ion track radius.

It can be clearly seen in Fig. 5(a) that the induced porosity in InSb is significantly higher than in GaSb. Even at the highest irradiation fluence for GaSb, which is four times the maximum fluence used for InSb, the measured swelling in the InSb thin film is almost three times higher. Swelling in InSb and GaSb thin films reaches different saturation values at higher fluences, which indicates that factors other than the ion fluence affect the swelling rate, such as vacancy diffusion. A previous report by Giulian *et al.* showed that the total thickness of a sputtered polycrystalline InSb film increases more than 16 times until it saturates after irradiation with 17 MeV Au ions at a fluence of 2×10^{14} ions/cm^2. The increased swelling in InSb is attributed to the creation of a cylindrical region around the ion path, where the mobility of atoms is heightened due to a local increase in the temperature. Vacancies accumulate to form voids that combine to reduce the surface energy, while interstitials diffuse away from the ion path.[2] In contrast to Ref. 2, an InSb sample in this study was in an amorphous phase after swift heavy ion irradiation.

Figure 5(b) shows the swelling of bulk InSb and GaSb samples measured using profilometry irradiated normal to the surface. GaSb swelling data were reproduced from Kluth *et al.*[18] They show that bulk InSb samples exhibit significantly greater swelling with a nonlinear growth rate in comparison with the swelling seen in bulk GaSb samples. Similar behavior has previously been attributed by Nitta *et al.* to larger void size and higher vacancy concentration in InSb compared with GaSb at comparable fluences, although in the low-energy irradiation regime, the material structures changed into polycrystalline after heavy ion irradiation.[7] Furthermore, irradiation-induced diffusion refers to the exchange of position between an atom and a vacancy due to irradiation. As a result, the rate of migration is heavily influenced by the concentration and distribution of vacancies. It is expected that the rate of irradiation-induced diffusion in InSb is faster than that in GaSb.[7]

For off-normal irradiation, it was difficult to conduct accurate measurements of swelling of InSb samples using SEM because of immense swelling and surface roughness. Further study and investigation are required to evaluate the swelling of InSb irradiated off-normal to the surface.

IV. SUMMARY AND CONCLUSIONS

In summary, the damage and microstructural characteristics of InSb after swift heavy ion irradiation with ^{197}Au have been examined and compared to earlier results on GaSb in terms of damage buildup and microstructural changes as a function of irradiation fluence ranging from 8.8×10^{10} to 5.6×10^{13} ions/cm^2. We found an ion track radius of about 16 ± 4 nm for normal incidence and 21 ± 6 nm for off-normal incidence, which is about 4–5 higher than that in GaSb. Moreover, the pore density was higher at off-normal irradiation than the irradiation normal to the surface. Furthermore, InSb shows a higher swelling rate than GaSb for the same irradiation conditions. Interestingly, the porosification process resulting from swift heavy ion irradiation requires much lower fluence than in the low-energy regime, almost 250 times lower to observe a similar porous structure in the low-energy regime. As previously seen in GaSb, for both InSb bulk and thin films, the material exhibits swelling above threshold fluence, which corresponds to almost complete amorphization of InSb samples.

AUTHOR DECLARATIONS
Conflict of Interest

The authors have no conflicts to disclose.

Author Contributions

Taleb Alwadi: Data curation (equal); Formal analysis (equal); Investigation (equal); Methodology (equal); Visualization (equal); Writing – original draft (equal). **Christian Notthoff:** Conceptualization (equal); Data curation (equal); Formal analysis (equal); Investigation (equal); Methodology (equal); Project administration (supporting); Supervision (equal); Visualization (supporting); Writing – review & editing (equal). **Shankar Dutt:** Investigation (supporting); Methodology (supporting); Writing – review & editing (equal). **Jessica Wierbik:** Methodology (supporting). **Nahid Afrin:** Methodology (supporting). **Alexander Kiy:** Methodology (supporting). **Patrick Kluth:** Conceptualization (equal); Formal analysis (supporting); Funding acquisition (lead); Investigation (equal); Methodology (equal); Project administration (lead); Resources (lead); Supervision (equal); Visualization (supporting); Writing – review & editing (lead).

DATA AVAILABILITY

The data that support the findings of this study are available from the corresponding author upon reasonable request.

REFERENCES

[1]C. S. Schnohr, P. Kluth, R. Giulian, D. J. Llewellyn, A. P. Byrne, D. J. Cookson, and M. C. Ridgway, Phys. Rev. B **81**, 075201 (2010).
[2]R. Giulian, J. B. Salazar, W. Just, D. J. Manzo, A. M. H. De Andrade, J. R. Schoffen, F. Bernardi, D. L. Baptista, and P. F. P. Fichtner, J. Phys. Appl. Phys. **50**, 485104 (2017).
[3]S. R. Das *et al.*, J. Appl. Phys. **116**, 083506 (2014).
[4]B. R. Bennett, R. Magno, J. B. Boos, W. Kruppa, and M. G. Ancona, Solid-State Electron. **49**, 1875 (2005).
[5]D. P. Datta, S. K. Garg, B. Satpati, P. K. Sahoo, A. Kanjilal, S. Dhara, D. Kanjilal, and T. Som, J. Appl. Phys. **116**, 143502 (2014).
[6]D. P. Datta and T. Som, Appl. Phys. Lett. **108**, 191603 (2016).
[7]N. Nitta, T. Hasegawa, H. Yasuda, Y. Hayashi, T. Yoshiie, M. Taniwaki, and H. Mori, Mater. Trans. **51**, 1004261067 (2010).
[8]N. Nitta, T. Hasegawa, H. Yasuda, K. Sato, Q. Xu, T. Yoshiie, M. Taniwaki, and A. Hatta, Radiat. Eff. Defects Solids **168**, 247 (2013).
[9]W. Wesch, E. Wendler, and C. S. Schnohr, Nucl. Instrum. Methods Phys. Res. B **277**, 58 (2012).
[10]L. M. Wang and R. C. Birtcher, Philos. Mag. A **64**, 1209 (1991).

[11]S. M. Kluth, D. Llewellyn, and M. C. Ridgway, Nucl. Instrum. Methods Phys. Res. B **242**, 640 (2006).

[12]T. Steinbach, C. S. Schnohr, P. Kluth, R. Giulian, L. L. Araujo, D. J. Sprouster, M. C. Ridgway, and W. Wesch, Phys. Rev. B **83**, 054113 (2011).

[13]G. Szenes, Z. E. Horvath, B. Pecz, F. Paszti, and L. Toth, Phys. Rev. B **65**, 045206 (2002).

[14]A. Kamarou, W. Wesch, E. Wendler, A. Undisz, and M. Rettenmayr, Phys. Rev. B **78**, 054111 (2008).

[15]J. F. Ziegler, M. D. Ziegler, and J. P. Biersack, Nucl. Instrum. Methods Phys. Res. B **268**, 1818 (2010).

[16]C. Notthoff, S. Jordan, A. Hadley, P. Mota-Santiago, R. G. Elliman, W. Lei, N. Kirby, and P. Kluth, Phys. Rev. Mater. **4**, 046001 (2020).

[17]J. F. Gibbons, Proc. IEEE **60**, 1062 (1972).

[18]P. Kluth *et al.*, Appl. Phys. Lett. **104**, 023105 (2014).

[19]D. Turnbull and M. H. Cohen, J. Chem. Phys. **34**, 120 (1961).

[20]W. J. Wright, T. C. Hufnagel, and W. D. Nix, J. Appl. Phys. **93**, 1432 (2003).

[21]A. E. Volkov and A. I. Ryazanov, J. Non-Cryst. Solids **117**, 256 (1990).

[22]C. Riedel and R. Spohr, Radiat. Eff. **42**, 69 (1979).

23 October 2023 20:14:17